Supporting Information

Direct synthesis of PtNi coated with Ni_3B for efficient electrochemical hydrogen evolution from seawater

Xiong Yang,[a] Yu-Xuan Xiao,[b] Fei Yu [a] Wen-Ying Zhao,[a] Ling Shen,[a] Jie Ying,[b] Song Zhang,[a] Kenneth I. Ozoemena,[c] Christoph Janiak,*[d] *Xiao-Yu Yang[ae]**

[a] *State Key Laboratory of Silicate Materials for Architectures & State Key Laboratory of Advanced Technology for Materials Synthesis and Processing & School of Chemistry, Chemical Engineering and Life Sciences & Laoshan Laboratory & School of Materials Science and Engineering & International School of Materials Science and Engineering, Wuhan University of Technology, Wuhan, 430070, China.*

[b]*School of Chemical Engineering and Technology, Sun Yat-sen University, Zhuhai, 519082, China.*

[c]*Molecular Sciences Institute, School of Chemistry, University of the Witwatersrand, Private Bag 3, Johannesburg 2050, South Africa.*

[d]*Institut für Anorganische Chemie und Strukturchemie, Heinrich-Heine-Universität Düsseldorf, Düsseldorf, 40204, Germany.*

[e]*National energy key laboratory for new hydrogen-ammonia energy technologies, Foshan Xianhu Laboratory, Foshan 528200, P.R.China*

* To whom correspondence should be addressed.
Email: xiaoyx63@mail.sysu.edu.cn (Y.X.X.); xyyang@whut.edu.cn (X.Y.Y.)

Experimental section

1. Materials.

H_2PtCl_6, $NiCl_2$, and polyvinylpyrrolidone (PVP, K30), were purchased from Shanghai Aladdin Biochemical Polytron Technologies Inc. Ethanol, KOH, NaCl, KBr, and $NaBH_4$ were purchased from Sinopharm Chemical Reagent Co., Ltd. Commercial Pt/C (20 wt.% Pt) was purchased from Johnson Matthey Corp. Commercial carbon black (Vulcan-XC 72R) was purchased from Shanghai Cabot Co., Ltd. All chemical reagents were used as received without further purification. De-ionized (DI) water (18.2 MΩcm) was used throughout.

2. Synthesis of $Pt_3Ni_{2-3x}@(Ni_3B)_x$.

In a typical synthesis, 120 mg of K30 was first dissolved in 30 mL of de-ionized water with magnetic stirring. Then, 3 mL of 2.5 mol L^{-1} KBr, 0.24 mL of 0.2 mol L^{-1} H_2PtCl_6 and 0.36 mL of 0.2 mol L^{-1} $NiCl_2$ were added to the solution in sequence. After stirring for 30 min, 36 mL of freshly prepared 2 mg mL^{-1} $NaBH_4$ aqueous solution was added dropwise to the mixed solution. After stirring for 20 min, the products were obtained through centrifugation and washing with de-ionized water for several times.

The Pt networks, Pt_3Ni networks, and $Pt_2Ni_{3-3x}@(Ni_3B)_x$ were prepared in the same way, by changing the volumes of the H_2PtCl_6 and $NiCl_2$ to 0.6mL and 0 mL for Pt networks, to 0.4 mL and 0.2 mL for Pt_3Ni networks, and to 0.15 mL and 0.45 mL for $Pt_2Ni_{3-3x}@(Ni_3B)_x$.

3. Fermi level calculation

For the calculation of Fermi level, the following equation was used. $\Phi = E_v - E_f$, where Φ refers to work function; E_v refers to vacuum level, 0 eV; E_f refers to Fermi level.

4. Electrochemical measurements

The as-prepared metals were dispersed 20 mL of ethanol, and 40 mg of support materials (Vulcan XC-72 carbon) to form well-dispersed suspensions. Then the mixture would stir for 12 h. The carbon-supported metals were collected through centrifugation (9,000 r.p.m. for 10 min) and dried in the vacuum drying oven (60 ℃) for 12 h.

The electrochemical measurements were performed at room temperature under an Autolab working station (Metrohm, Switzerland) using a glassy carbon electrode. Before measurements, the catalyst dispersion or ink was prepared by mixing a certain amount of catalyst in 880 μL of isopropanol, 100 μL of de-ionized water and 20 μL of 5 wt.% Nafion solution followed by ultrasonication for 30 min. The Pt loading of all samples on glassy carbon was 3 μg. An Ag/AgCl electrode and a graphite rod (99.99%) were used as the reference and the counter electrode.

For the electrochemically active surface area (ECSA) study, cyclic voltammetry (CV) was conducted over a potential range from 0.05 V to 1.20 V versus a reversible hydrogen electrode (RHE) at a scan rate of 50 mV s^{-1} in 1 mol L^{-1} KOH and alkaline seawater (3.5 at.% NaCl + 1 mol L^{-1} KOH). ECSA values were calculated by integrating the area under the curve for the hydrogen adsorption/desorption region between 0.05 and 0.40 V (vs. RHE) for the reverse sweep in the cyclic voltammetry.

Polarization curves were collected in alkaline media alkaline seawater at a rotation rate of 1600 rpm with a sweep rate of 5 mV s^{-1}. Chronopotentiometric measurements were performed in alkaline seawater at 10 mA/cm^2 and 100 mA/cm^2 for 20 h, respectively. Electrochemical impedance spectroscopy (EIS) measurements were carried out in the frequency range from 100 kHz to 0.1 Hz with an AC amplitude of 10 mV. All potentials are presented with reference to the RHE without insulation resistance (iR) compensation.

The turnover frequency (TOF) of catalysts was calculated according to the following formula.

$$TOF = \frac{j(\eta)\cdot A\cdot \frac{N_A}{n\cdot F}}{S}$$

Where j(η) is the current density (A cm^{-2} electrode) at an overpotential of η (70 mV); A is the superficial electrode area (0.196 cm^2); N_A is the Avogadro number, 6.02×10^{23} (mol^{-1}); n is the number of electrons transferred per molecule, 2 for HER; F is the Faraday constant, 96485 (C mol^{-1} electrons); S is the number of active sites. To avoid the calculation difficulties, all the metal atoms in the catalysts were assumed as active sites, which can be determined according to ICP-AES results.

5. Preparation of RuO_2-300/carbon cloth (CC) electrode

Anode: RuO_2 was obtained as previously reported.[1] The commercial CC (1 × 1.5 cm^2) was cleaned by ultrasonication with ethanol and ultrapure de-ionized water for several minutes. Then 200 μL of catalyst ink (1 mg of Ru-300) was dropped onto the CC (1 × 1.5 cm^2, each time with 20 μL for 10 times). The catalyst/CC electrodes were dried at room temperature for 12 h.

Cathode: The Pt networks/CC electrode, Pt_3Ni networks/CC electrode, $Pt_3Ni_{2-3x}@(Ni_3B)_x$/CC electrode, and $Pt_2Ni_{3-3x}@(Ni_3B)_x$/CC electrode were prepared in the same way, by changing the volume of the ink to 3.33 mL (1 mg of Pt).

6. Characterization.

Scanning electron microscopy (SEM) images were obtained by an S-4800 electron microscope (HITACHI). Transmission electron microscopy (TEM), high-angle annular dark field scanning transmission electron microscopy (HAADF-STEM), and energy-dispersive X-ray spectroscopy (EDX) analyses were conducted with a Talos F200S (Thermo Fisher, USA) in Wuhan University of Technology. X-ray diffraction (XRD) measurements were performed on a Bruker D8-Advance X-ray diffractometer operating with Cu Kα radiation (λ=1.54056 Å). The nitrogen physisorption isotherms were measured on a Micromeritics ASAP 3020 system, and samples were degassed for 12 h at 60 °C under vacuum before the measurements. The X-ray photoelectron spectroscopy (XPS) measurements and ultraviolet photoelectron spectroscopy (UPS) were carried out by an ESCALAB 250Xi (Thermo Fisher, USA). Electron spin resonance (ESR) measurements were performed at the X-band using a JEOL FA 2000 spectrometer. The content analyses of Pt, Ni, and Cu were measured by inductively coupled plasma-atomic emission spectrometry (ICP-AES, Prodigy 7, LEEMAN LABS INC, USA).

7. Density functional theory (DFT) calculations

All calculations were performed using the Vienna ab initio simulation package (VASP).[2] The Perdew-Burke-Ernzerhof (PBE) functional within the generalized gradient approximation

(GGA) was utilized to express electron exchange correlation,[3] and the projector augmented wave (PAW) method was applied to describe the pseudo-potentials.[4] Dispersion-corrected DFT-D3 schemes were employed to describe possible van der Waals (vdW) interaction.[5] The energy cut-off for the plane-wave basis was set to 450 eV. The Brillouin zone in reciprocal space was sampled using the Monkhorst-Pack scheme with 3 × 3 × 1 k-point grids for geometry optimization. All structures were fully relaxed until the forces were smaller than 0.02 eV $Å^{-1}$, and the convergence threshold in electronic relaxation was set to 10^{-5} eV using the conjugate gradient algorithm.

To understand fully the reaction mechanism of $Pt_3Ni_{2-3x}@(Ni_3B)_x$, we have made a special model to simulate $Pt_3Ni_{2-3x}@(Ni_3B)_x$. For the simulation of the low crystalline Ni_3B model, we used the "Heterogeneous Cell Module" in Materials Studio to build the low crystalline Ni_3B model. After running of ab initio molecular dynamics at 300 K with full relaxation up to 2 ps, we randomly chose a snap as a heterogeneous model used to form the heterostructure with Pt_3Ni, a vacuum layer larger than 20 Å in the z direction was set to prevent the interaction between periodic images. The Pt (111) slab model, Ni (111) slab model, and Pt_3Ni (111) was built as a reference to show the performance of the $Pt_3Ni_{2-3x}@(Ni_3B)_x$ system for HER. For both systems, the bottom 4 atomic layers need to be fixed during the structural relaxation.

According to the reaction environment, the reaction pathway is more likely as follows:

$$H_2O + * \rightarrow H_2O* \quad (1)$$

$$H_2O* \rightarrow H* + OH* \quad (2)$$

$$e^- + H* + OH* \rightarrow H* + OH^- \quad (3)$$

$$H* \rightarrow 1/2\ H_2 \quad (4)$$

where * indicates reaction sites.

The Gibbs free-energy (ΔG_{ads}) is evaluated as follows:

$$\Delta G_{ads} = \Delta E_{ads} + \Delta ZPE - T\Delta S$$

where ΔE_{ads} is the adsorption energy of adsorbates, such as the H_2O molecule absorbed on the surface, and ΔZPE is the zero-point-energy difference between the adsorbates absorbed on the surface and in the gas phase. T is the temperature and the entropy change (ΔS) of each adsorbed state were calculated according to the standard molar Gibbs energy of formation at 298.15 K. the adsorption energy (ΔE_{ads}) is defined as follows:

$$\Delta E_{ads} = E_{total} - E_{slab} - E_{gas}$$

Where E_{total} is the total energy of the given system with the adsorbates on the surface, E_{slab} is the energy of the bare model, and E_{gas} is the energy of the adsorbate's gas energy.

In addition, the energy of Cl^- is hardly obtained through DFT calculation. In order to calculate the Gibbs free-energy of Cl^- adsorbed on catalysts, we use the follow method.

$$* + Cl^- \rightarrow Cl* + e^- \quad (5)$$

$$\Delta G_1 = G(Cl*) + G(e^-) - G(*) - G(Cl^-)$$

$$* + H^+ + Cl^- \rightarrow Cl* + (H^+ + e^-) \quad (6)$$

$$\Delta G_2 = G(Cl*) + [G(H^+) + G(e^-)] - G(*) - G(H^+) - G(Cl^-)$$

$$* + HCl\ (g) \rightarrow Cl* + (H^+ + e^-) \quad (7)$$

$$\Delta G_3 = G(Cl*) + [G(H^+) + G(e^-)] - G(*) - G(HCl)$$

$$HCl\ (g) \rightarrow H^+ + Cl^-\ (aq) \quad (8)$$

$$\Delta G_4 = G(H^+) + G(Cl^-) - G(HCl)$$

ΔG_4 can be found in the CRC HANDBOOK of CHEMISTRT and PHYSICS. Hence, ΔG_1 can be obtained by:

$$\Delta G_1 = \Delta G_3 - \Delta G_4$$

Supporting data

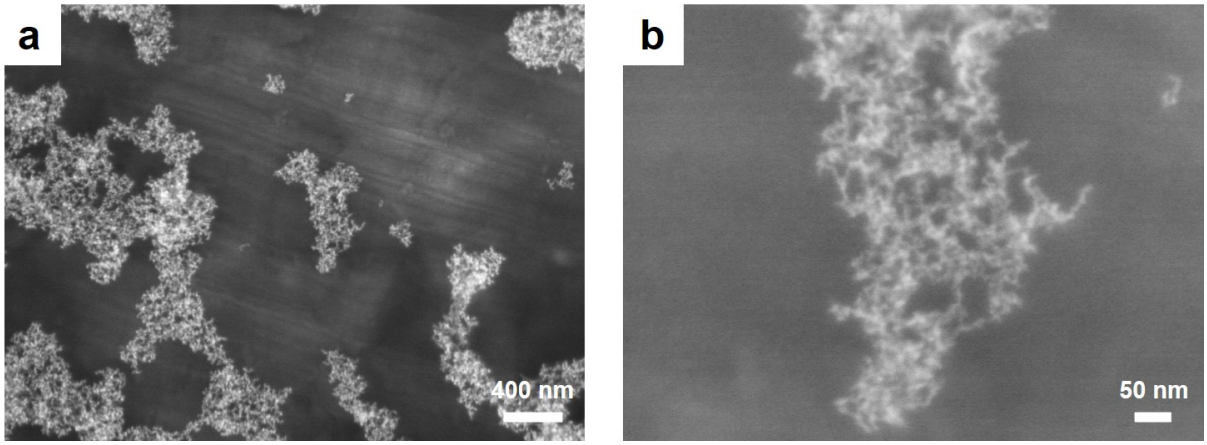

Figure S1. (a) Low and (b) high magnification SEM image of Pt networks.

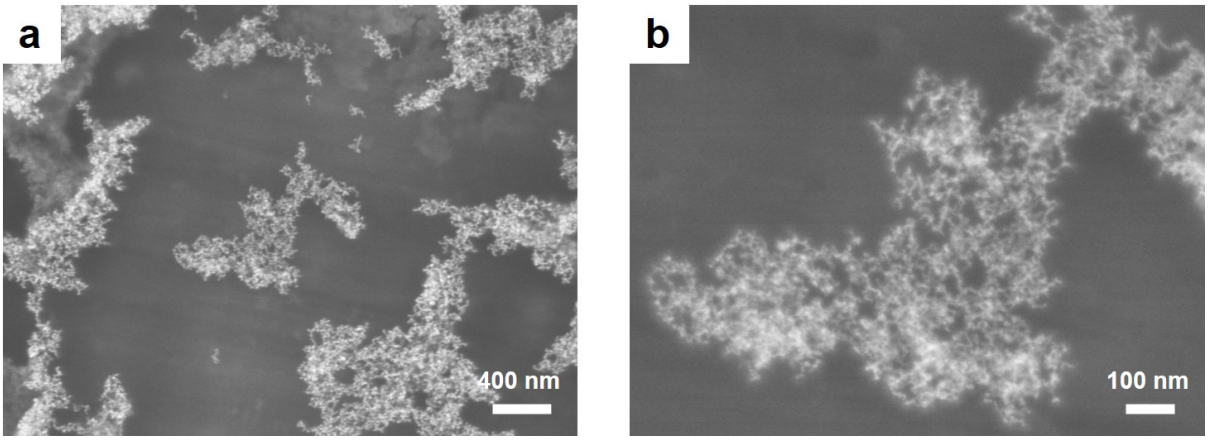

Figure S2. (a) Low and (b) high magnification SEM image of Pt_3Ni networks.

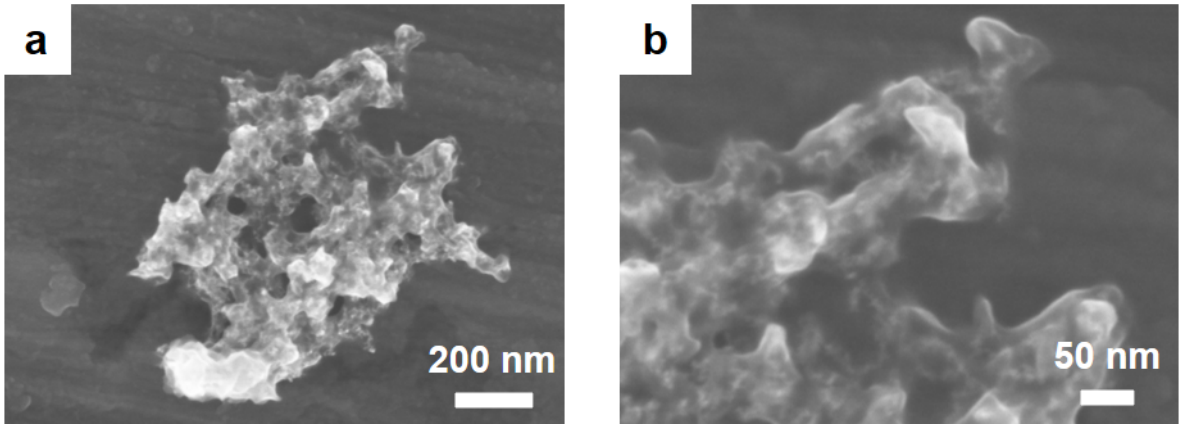

Figure S3. (a) Low and (b) high magnification SEM image of $Pt_3Ni_{2-3x}@(Ni_3B)_x$.

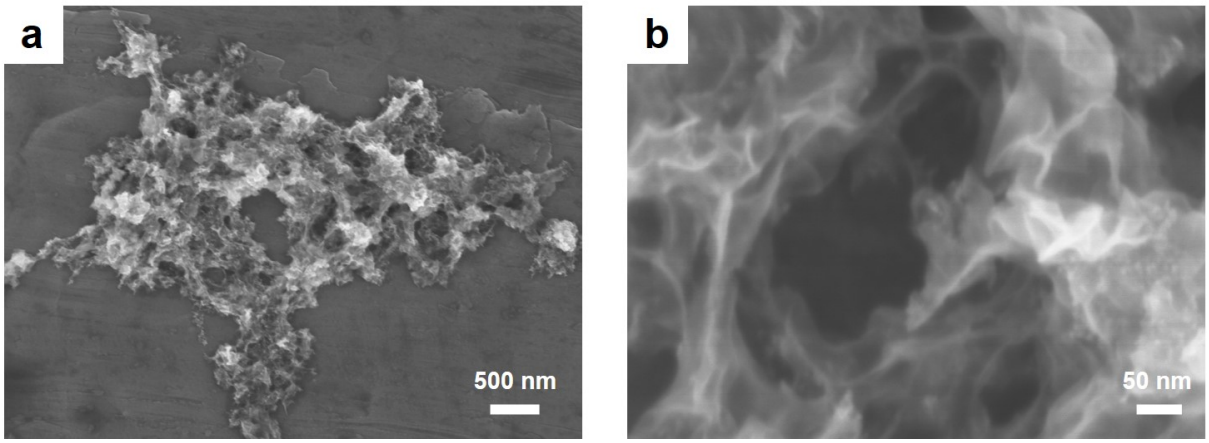

Figure S4. (a) Low and (b) high magnification SEM image of $Pt_2Ni_{3-3x}@(Ni_3B)_x$.

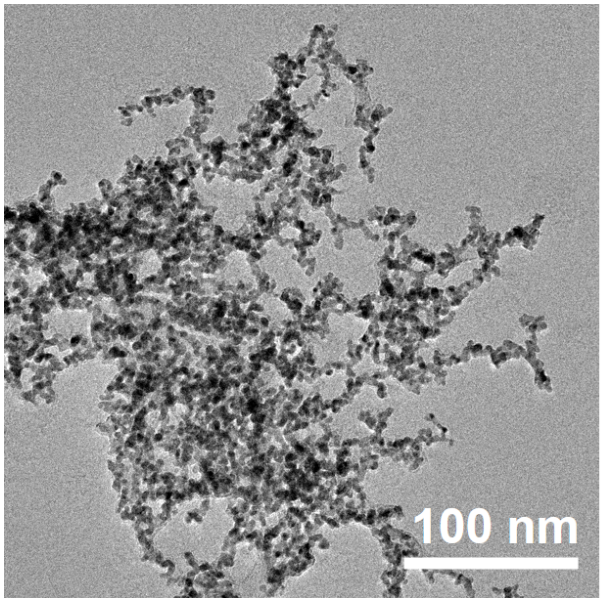

Figure S5. Low magnification TEM images of Pt_3Ni.

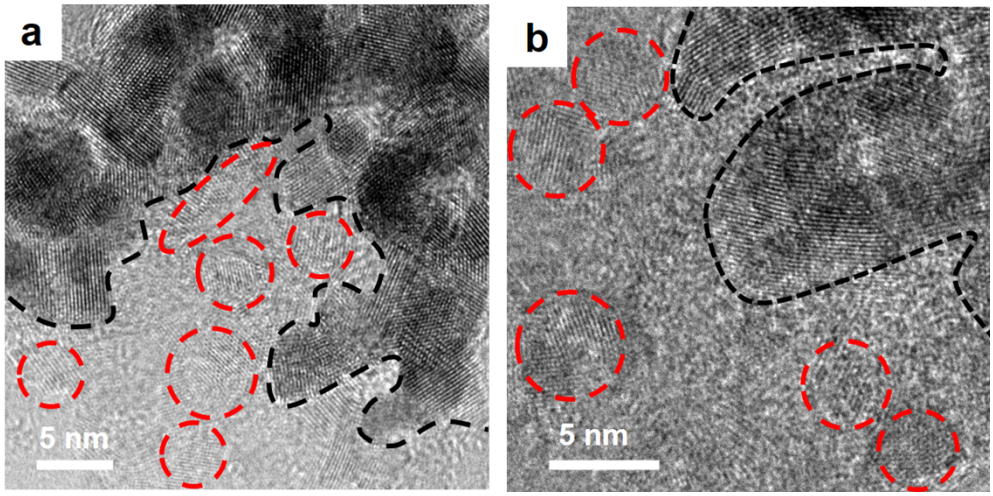

Figure S6. High magnification TEM images of $Pt_3Ni_{2-3x}@(Ni_3B)_x$ with heterojunction structure.

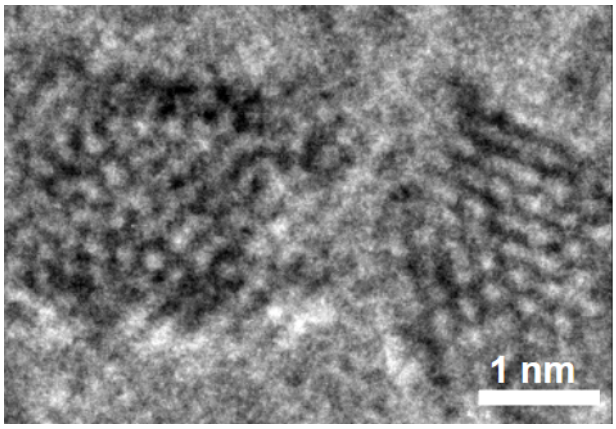

Figure S7. High magnification TEM images of $Pt_3Ni_{2-3x}@(Ni_3B)_x$

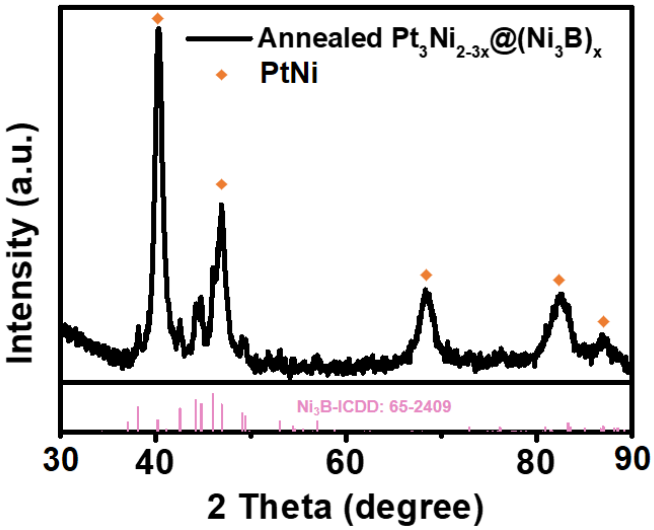

Figure S8. XRD patterns of annealed $Pt_3Ni_{2-3x}@(Ni_3B)_x$

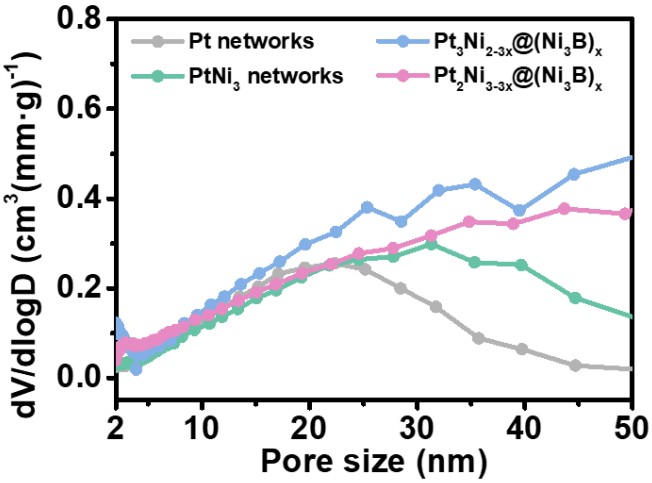

Figure S9. Pore size distributions of Pt networks, Pt_3Ni networks, $Pt_3Ni_{2-3x}@(Ni_3B)_x$, and $Pt_2Ni_{3-3x}@(Ni_3B)_x$.

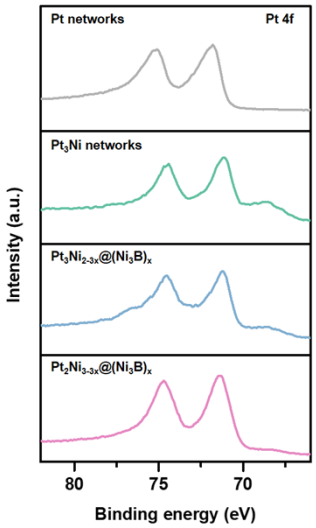

Figure S10. XPS spectra showing the Pt 4f region for Pt networks, Pt_3Ni networks, $Pt_3Ni_{2-3x}@(Ni_3B)_x$, and $Pt_2Ni_{3-3x}@(Ni_3B)_x$.

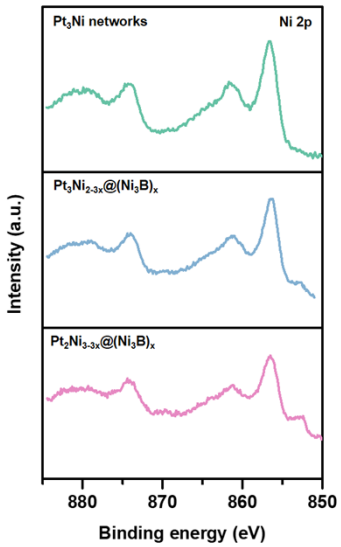

Figure S11. XPS spectra showing the Ni 2p region for Pt_3Ni networks, $Pt_3Ni_{2-3x}@(Ni_3B)_x$ and $Pt_2Ni_{3-3x}@(Ni_3B)_x$.

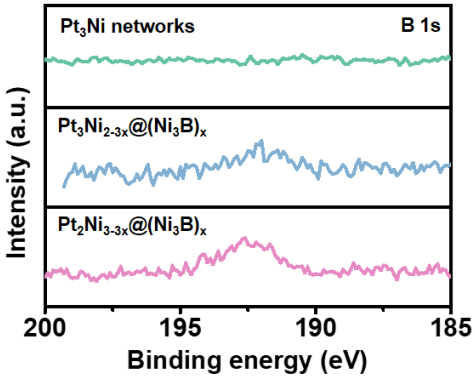

Figure S12. XPS spectra showing the B 1s region for Pt networks, $Pt_3Ni_{2-3x}@(Ni_3B)_x$ and $Pt_2Ni_{3-3x}@(Ni_3B)_x$.

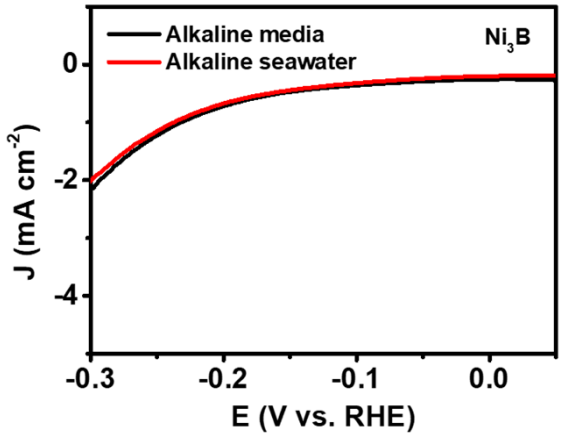

Figure S13. HER polarization curves of Ni_3B in alkaline media and alkaline seawater.

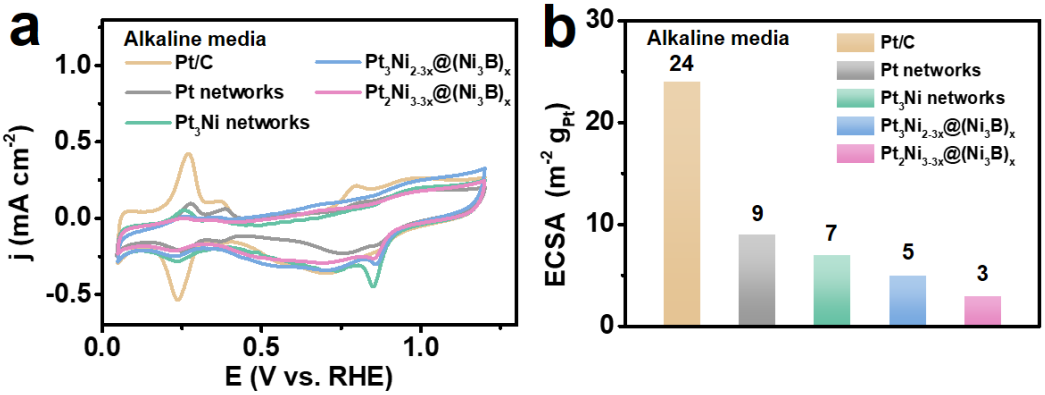

Figure S14. (a) CV curves and (b) ECSA of commercial Pt/C, Pt networks, Pt_3Ni networks, $Pt_3Ni_{2-3x}@(Ni_3B)_x$, and $Pt_2Ni_{3-3x}@(Ni_3B)_x$ in alkaline media.

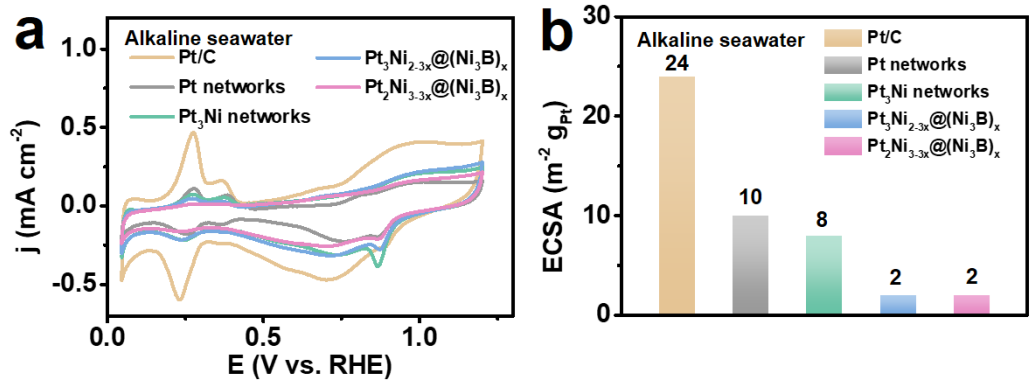

Figure S15. (a) CV curves and (b) ECSA of commercial Pt/C, Pt networks, Pt_3Ni networks, $Pt_3Ni_{2-3x}@(Ni_3B)_x$, and $Pt_2Ni_{3-3x}@(Ni_3B)_x$ in alkaline seawater.

To confirm the electrochemically active surface area (ECSA) of $Pt_3Ni_{2-3x}@(Ni_3B)_x$, the cyclic voltammetry (CV) curves of different samples in N_2-saturated (Figure S11) alkaline media and (Figure S12) alkaline seawater were obtained, the signals of which are mainly due to the Pt-based alloy (111) and (100) ordered domains. Note that specific ECSAs of Pt/C is higher than those of other catalysts due to the small particle size. As a consequence of covered Ni_3B onto the active sites of PtNi networks, both of $Pt_3Ni_{2-3x}@(Ni_3B)_x$ and $Pt_2Ni_{3-3x}@(Ni_3B)_x$ shows the smaller ECSAs. The HER performances of these Pt-based catalysts were also evaluated.

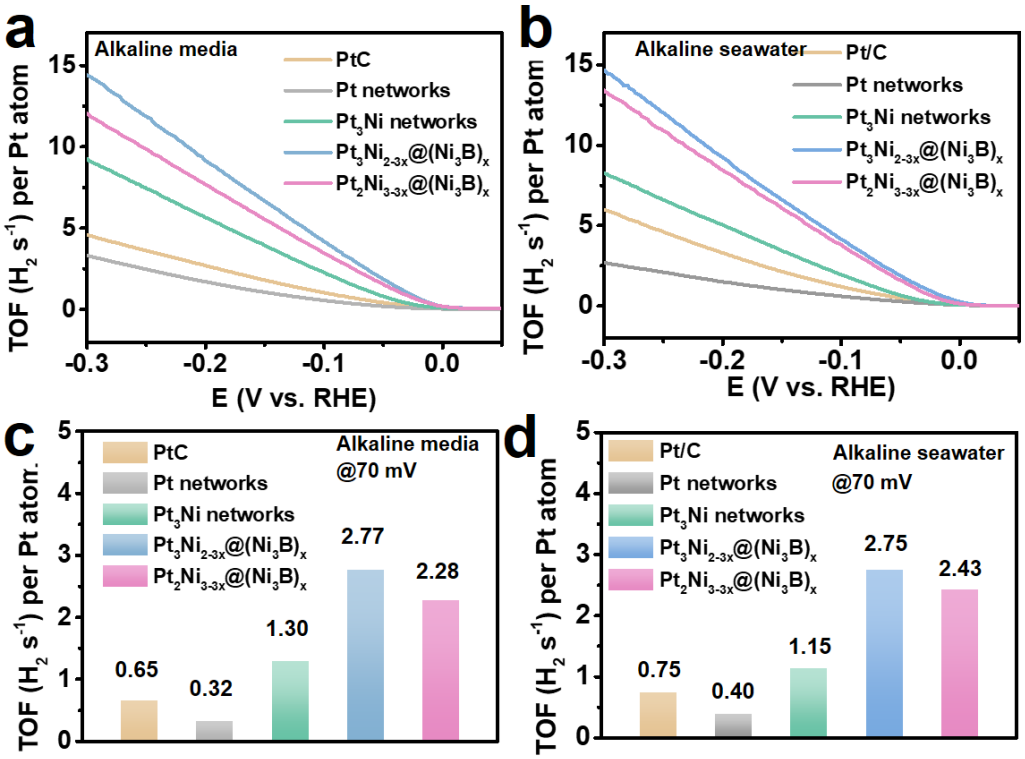

Figure S16. Calculated TOF curves of commercial Pt/C, Pt networks, Pt_3Ni networks, $Pt_3Ni_{2-3x}@(Ni_3B)_x$, and $Pt_2Ni_{3-3x}@(Ni_3B)_x$ in (a) alkaline media, (b) alkaline seawater and the corresponding TOF values at 0.07 V in (c) alkaline media and (d) alkaline seawater.

As shown in Figure S13, the intrinsic activity of $Pt_3Ni_{2-3x}@(Ni_3B)_x$ was further evaluated by determining the HER turnover frequencies (TOF). $Pt_3Ni_{2-3x}@(Ni_3B)_x$ exhibits the highest TOF values in both (Figure S13c) alkaline media and (Figure S13h) alkaline seawater. Specifically, it has the highest TOF value of 2.77 s^{-1} in alkaline media and 2.75 s^{-1} in alkaline seawater, which is 9-fold and 7-fold higher than that of Pt/C in alkaline media and alkaline seawater, respectively.

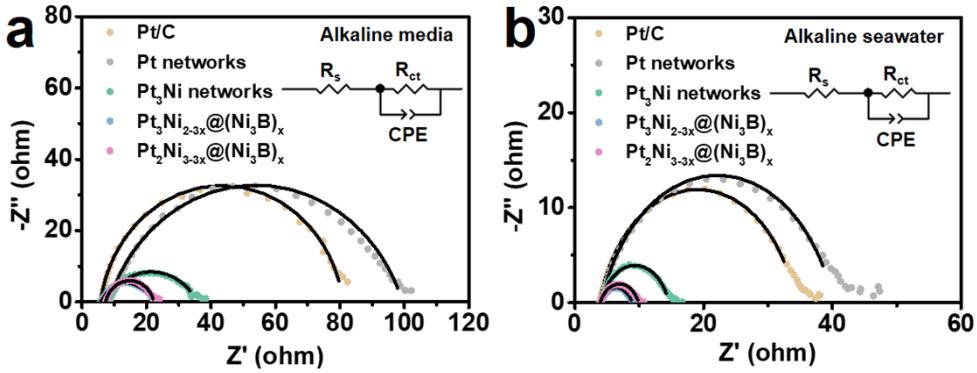

Figure S17. Nyquist plots and analog circuit of Pt/C, Pt networks, Pt_3Ni networks, $Pt_3Ni_{2-3x}@(Ni_3B)_x$, and $Pt_2Ni_{3-3x}@(Ni_3B)_x$ in (a) alkaline media and (b) alkaline seawater.

Electrochemical impedance spectroscopy (EIS) at -50 mV was carried out (Figure S14) to further investigate the interface charge transfer. $Pt_3Ni_{2-3x}@(Ni_3B)_x$ delivers the lowest charge transfer resistance and highest conductivity, compared to the other electrocatalysts during HER in alkaline media and alkaline seawater.

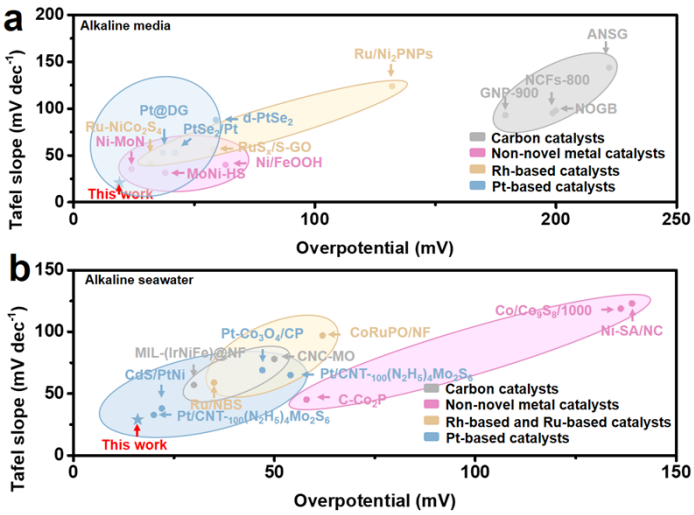

Figure S18. Performance of $Pt_3Ni_{2-3x}@(Ni_3B)_x$ in comparison to other catalysts towards HER in (a) alkaline media and (b) alkaline seawater.

A comparison of overpotential and Tafel slopes indicates that the HER performance of $Pt_3Ni_{2-3x}@(Ni_3B)_x$ in both of alkaline media(Figure S15a) and alkaline seawater (Figure S15b) is not only higher than those of the other prepared catalysts, but also superior to those of other previously reported electrocatalysts.

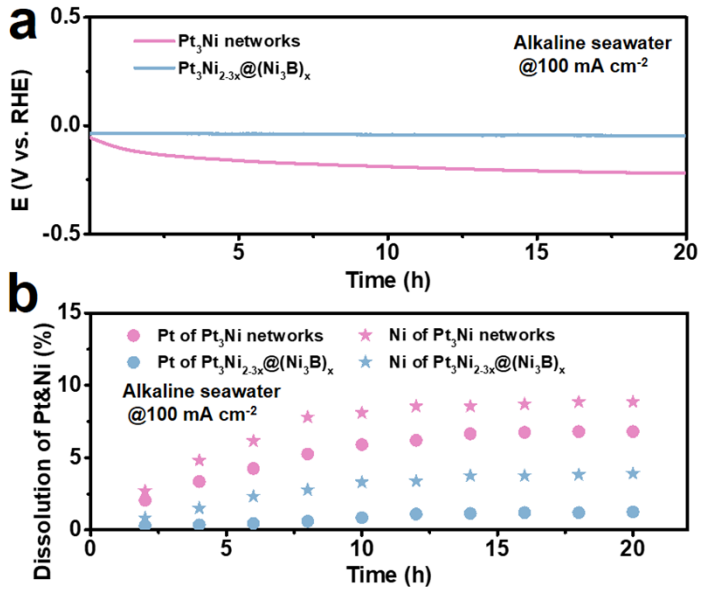

Figure S19. (a) Chronopotentiometry of Pt_3Ni networks and $Pt_3Ni_{2-3x}@(Ni_3B)_x$ under the current density of 100 mA cm^{-2} in alkaline seawater and (b) corresponding ICP analysis of the dissolution of Pt and Ni

To further investigate the corrosion process in alkaline seawater, Pt_3Ni and $Pt_3Ni_{2-3x}@(Ni_3B)_x$ displayed long-term stability with high current density (100 mA cm^{-2}) and Pt mass (1 mg) in alkaline seawater (Figure S16a). Additionally, the ICP-AES was texted to monitor the amount of dissolved Pt and Ni during the process (Figure S16b and Table S8). It is obvious that Ni shows a higher dissolution rate than Pt in Pt_3Ni, which may come from the electrochemical corrosion in which the Ni acts as the cathode due to the electron transfer from Ni to Pt. Benefiting from the covered protective electron-rich Ni_3B coating, $Pt_3Ni_{2-3x}@(Ni_3B)_x$ shows a lower dissolution of Ni and Pt, revealing the higher resistance of $Pt_3Ni_{2-3x}@(Ni_3B)_x$.

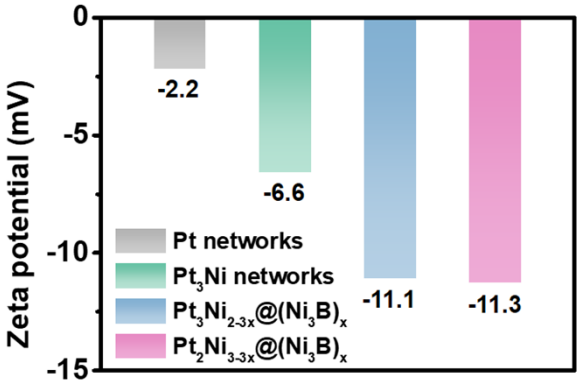

Figure S20. Zeta potential measurements for Pt networks, Pt_3Ni networks, $Pt_3Ni_{2-3x}@(Ni_3B)_x$ and $Pt_2Ni_{3-3x}@(Ni_3B)_x$.

The Zeta potential in neutral saline water (3.5 wt.% NaCl) was utilized to investigate the overpotential over the diffusion layer The negative Zeta potential of $Pt_3Ni_{2-3x}@(Ni_3B)_x$ (-11.1 mV) confirms the negative charge on the surface of $Pt_3Ni_{2-3x}@(Ni_3B)_x$ surface owing to the directed electron transfer. Notably, $Pt_3Ni_{2-3x}@(Ni_3B)_x$ (-11.1 mV) shows a more negative potential compared to Pt networks (-2.2 mV) and PtNi networks (-6.6 mV), helping to avoid the agglomeration of nanoparticles and resulting in a higher stability. All these results definitely confirm that $Pt_3Ni_{2-3x}@(Ni_3B)_x$ has both excellent activity and durability towards HER, due to the electron-rich surface of Ni_3B.

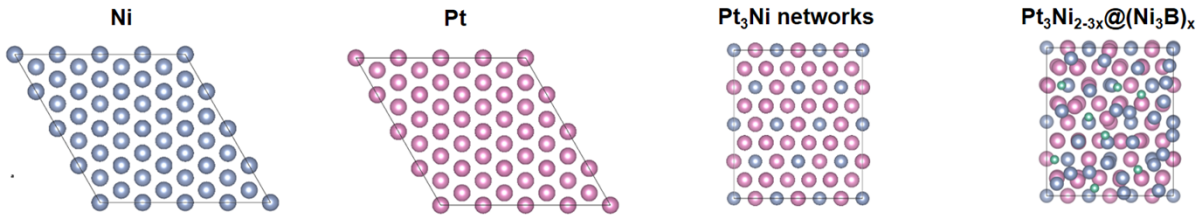

Figure S21. The results of the DFT calculations and the corresponding mechanisms of the electrocatalytic HER on the surfaces of different catalysts under alkaline conditions.

To elucidate the inherent relationship between the electronic structure and the excellent electrocatalytic HER performance of $Pt_3Ni_{2-3x}@(Ni_3B)_x$, density functional theory (DFT) calculations were performed on the electrocatalyst models including the (111) facet of the Ni, Pt networks, Pt_3Ni networks and $Pt_3Ni_{2-3x}@(Ni_3B)_x$ (Figure 5a). In order to further understand the alkaline HER mechanism, we have proceeded to construct the models for adsorption of intermediates on the surface.

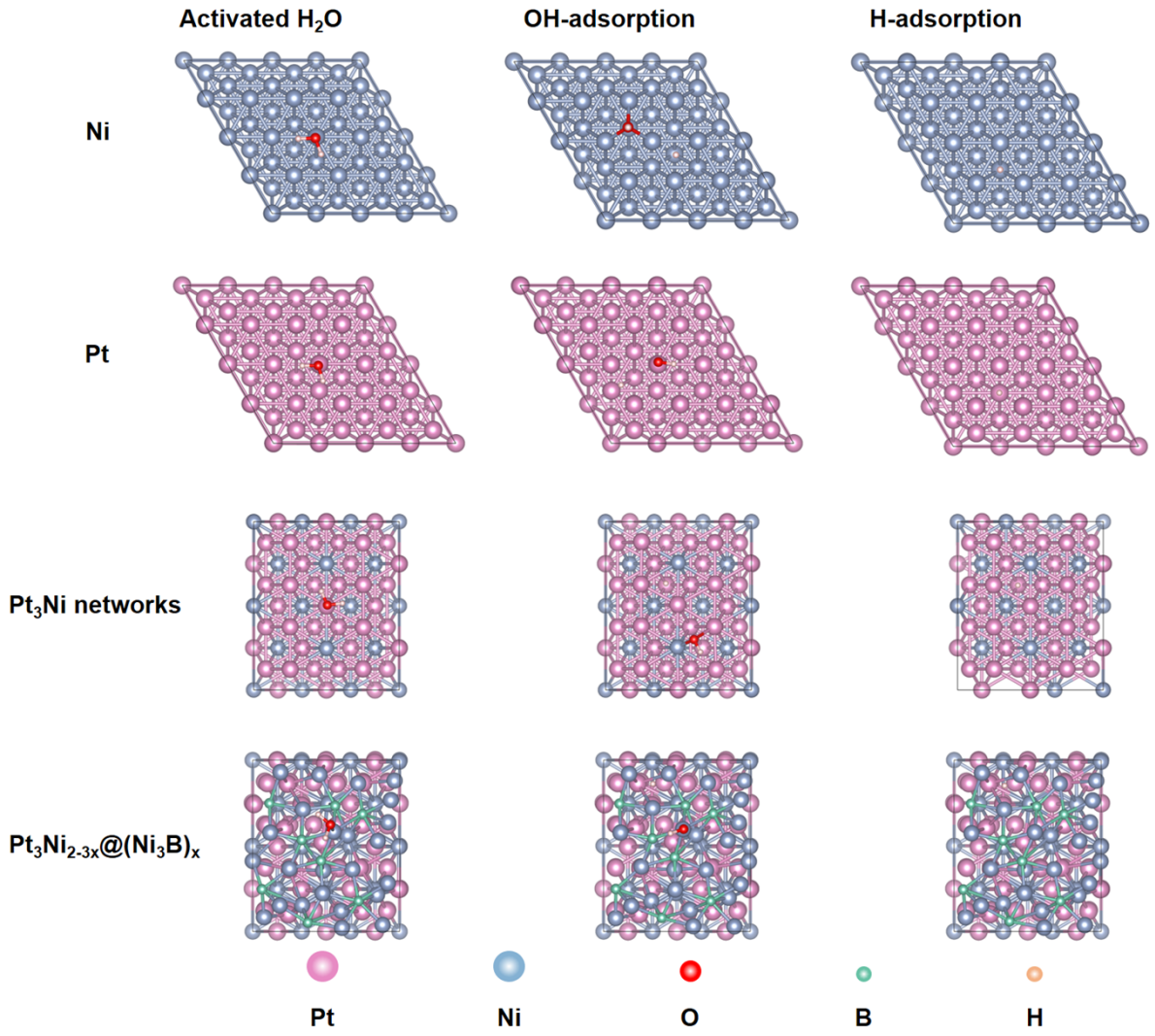

Figure S22. Structural models of activated H_2O adsorption, OH adsorption, and H adsorption of Pt, Ni, Pt_3Ni networks, and $Pt_3Ni_{2-3x}@(Ni_3B)_x$.

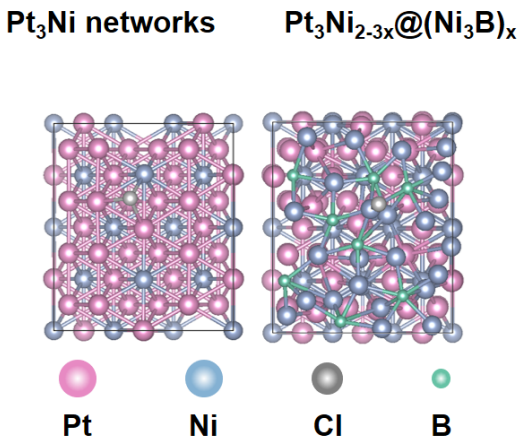

Figure S23. Structural models of Cl^- adsorption of Pt_3Ni networks and $Pt_3Ni_{2-3x}@(Ni_3B)_x$.

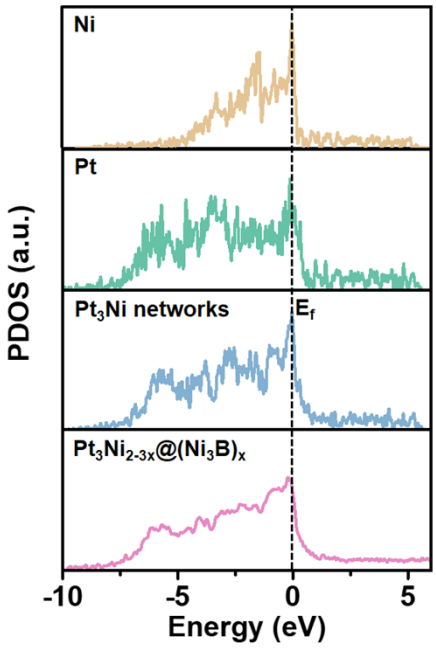

Figure S24. PDOS of Ni, Pt networks, Pt_3Ni networks, and $Pt_3Ni_{2-3x}@(Ni_3B)_x$.

Figure S21 shows the partial density of states (PDOS) diagrams for the four models of Ni, Pt, Pt_3Ni networks, and $Pt_3Ni_{2-3x}@(Ni_3B)_x$. The d-band center follows the sequence as Ni (-1.34 eV) > $Pt_3Ni_{2-3x}@(Ni_3B)_x$ (-2.13 eV) > Pt_3Ni networks(-2.24 eV) > Pt (-2.50 eV). The appropriate d-band center of $Pt_3Ni_{2-3x}@(Ni_3B)_x$ avoids the strong adsorption and desorption to intermediates which is harmful to a catalytic HER reaction.

Table S1. ICP-AES data of Pt_3Ni networks, $Pt_3Ni_{2-3x}@(Ni_3B)_x$ and $Pt_2Ni_{3-3x}@(Ni_3B)_x$.

Sample	Pt (at.%)	Ni (at.%)	B (at.%)
Pt_3Ni	75	25	N.A.
$Pt_3Ni_{2-3x}@(Ni_3B)_x$	63	33	4
$Pt_2Ni_{3-3x}@(Ni_3B)_x$	38	55	7

Table S2: Comparison of the specific surface area of $Pt_3Ni_{2-3x}@(Ni_3B)_x$ with porous metals.

Number	Metal	Specific surface area (m^2/g)	Reference
1	$Pt_3Ni_{2-3x}@(Ni_3B)_x$	169	This work
2	$Pt_2Ni_{3-3x}@(Ni_3B)_x$	91	This work
3	Pt_3Ni networks	60	This work
4	Pt networks	55	This work
5	PtPdCu-HS	107	Nano Lett. 2021, 21, 7870-7878
6	PtPdCu-S	46	
7	PtCu dendrites	6	Sens. Actuators B-Chem. 2016, 230, 721-730.
8	CuSe dendrites	6	ACS Sustainable Chem. Eng. 2017, 5, 4154-4160.
9	CoNi dendrites	57	Appl. Catal. B-Environ. 2019, 254, 634-646.
10	Pd-Cu network	21	Int. J. Hydrog. Energy 2016, 41, 6773-6780.
11	Pt spheres	36	Chem. Commun. 2011, 47, 3885-3887.
12	Pt-Cu tetradecahedrons	69	CrystEngComm. 2019, 21, 1903-1909.
13	Pd-Cu nanopheres	18	ACS Appl. Mater. Interfaces. 2016, 8, 30948-30955.
14	PtCu nanotubes	22	Energy Environ. Sci. 2017, 10, 1751-1756.
15	PtPd nanoparticles	53	J. Am. Chem. Soc. 2013, 135, 16762-16765.
16	PtPdCu spheres	64	J. Mater. Chem. A 2015, 3, 18053-18058.
17	Pd spheres	61	Angew. Chem. Int. Ed. 2013, 52, 2520-2524.
18	PtCu nanocrystals	54	Nanoscale 2015, 7, 16860-16866.
19	PdAu networks	105	Angew. Chem. Int. Ed. 2018, 57, 2963-2966.
20	Pt nanoparticles	39	J. Am. Chem. Soc. 2011, 133, 14526-14529.

Table S3. Peak fitting results of Pt 4f and Ni 2p signals for Pt/C, Pt networks, Pt_3Ni networks, $Pt_3Ni_{2-3x}@(Ni_3B)_x$, and $Pt_2Ni_{3-3x}@(Ni_3B)_x$.

Sample	B.E. of Pt $4f_{7/2}$ (eV)	B.E. of Pt $4f_{5/2}$ (eV)	B.E. of Ni^{2+} $2p_{3/2}$ (eV)	B.E. of Ni^{2+} $2p_{1/2}$ (eV)
Pt networks	71.8	75.2	N.A.	N.A.
Pt_3Ni networks	71.1	74.4	856.8	874.4
$Pt_3Ni_{2-3x}@(Ni_3B)_x$	71.3	74.5	856.6	874.3
$Pt_2Ni_{3-3x}@(Ni_3B)_x$	71.5	74.7	856.5	874.2

N.A. = not applicable

Table S4. Electrochemical test results of Pt/C, Pt networks, Pt_3Ni networks, $Pt_3Ni_{2-3x}@(Ni_3B)_x$, and $Pt_2Ni_{3-3x}@(Ni_3B)_x$.

Sample	Alkaline seawater		1 M KOH	
	Overpotential at 10 mA/cm² (η_{10}, mV)	TOF (H^2 s^{-1})	Overpotential at 10 mA/cm² (η_{10}, mV)	TOF (H^2 s^{-1})
Pt/C	63	0.75	70	0.65
Pt networks	106	0.40	110	0.32
Pt_3Ni networks	29	1.76	30	1.50
$Pt_3Ni_{2-3x}@(Ni_3B)_x$	16	2.75	19	2.77
$Pt_2Ni_{3-3x}@(Ni_3B)_x$	24	2.43	24	2.28

Table S5. Performance of $Pt_3Ni_{2-3x}@(Ni_3B)_x$ in comparison to other catalysts towards HER in 1 M KOH.

Catalyst	Overpotential (mV@10 mA cm^{-2})	Tafel slope (mV dec^{-1})	Reference
$Pt_3Ni_{2-3x}@(Ni_3B)_x$	19	21	This work
PdCo-Co_3S_4	96	22.23	Adv. Sci. 2024, e2309927.
Ni-MoN	24	35.5	Adv. Mater. 2022, 34, e2201774.
$PtSe_2$/Pt	42	53	Angew. Chem. Int. Ed. 2021,60, 23388-23393.
Ni@N-HCGHF	95	57	Adv. Mater. 2020, 32, e2003313.
ANSG	222	143.7	J. Colloid. Interface Sci. 2020, 577, 101-108.
Ru/Ni_2PNPs	132	124	ACS Sustain. Chem. Eng. 2019, 7, 17714-17722.
Pt@DG	37	53	J. Am. Chem. Soc. 2022, 144, 2171-2178.
d-$PtSe_2$	59	88	Adv. Energy Mater. 2022, 12, 2102359.
Ru-$NiCo_2S_4$	32	41.3	Adv. Funct. Mater. 2021, 32, 2109731.
GNP-900	179	93	Appl. Surf. Sci. 2021, 544, 148912.
NOGB	200	98	Adv. Energy Mater. 2019, 9, 1803867.
NCFs-800	198.6	95.2	Int. J. Hydrogen Energy 2020, 45, 4035-4042.
Ni/FeOOH	63	40	Adv. Energy Mater. 2020, 10, 1904020.
RuS_x/S-GO	58	56	Small 2019, 15, e1904043.
MoNi-HS	38	31.4	ACS Appl. Mater. Interfaces 2019, 11, 21998-22004.

Table S6. Performance of $Pt_3Ni_{2-3x}@(Ni_3B)_x$ in comparison to compared catalysts towards HER in alkaline seawater.

Catalyst	Electrolytes	Overpotential (mV@10 mA cm^{-2})	Tafel slope (mV dec^{-1})	Reference
$Pt_3Ni_{2-3x}@(Ni_3B)_x$	1 mol/L KOH + 0.5 mol/L NaCl	16	29	This work
MIL-(IrNiFe)@NF	1 mol/L KOH + 0.5 mol/L NaCl	~30	57	J. Mater. Chem. A 2021, 9, 27424-27433.
NiPx@HA	1.0 M KOH + 0.5 M NaCl	52	98.12	Small 2022, 19, 2205689.
Pt-Co_3O_4/CP	1 mol/L NaOH + 3.5 at.% NaCl	47	69	J. Mater. Chem. A 2021, 9, 6316-6324.
	mimic alkaline	54	65	
CNC-MO	1 mol/L KOH + 0.5 mol/L NaCl	~50	78	Nano Energy 021, 87, 106160.
C-Co_2P	1 mol/L KOH+ 0.5 mol/L NaCl	58	45.1	Adv. Funct. Mater. 2021, 31, 2107333.
CoRuPO/NF	1 mol/L KOH + seawater	62	97	RSC Adv. 2020, 10, 27235-27241.
Ru/NBS	1 M KOH + seawater	35	58.9	Electrochem. Commun. 2020, 111, 106647.
Ni-SA/NC	1 mol/L KOH + seawater	139	123	Adv. Mater. 2021, 33, e2003846.
$Pt_2/Ni(OH)_2$/NF	1 mol/L KOH + seawater	19	70	A ppl. Catal. B-environ. 2023, 331, 122703.
CdS/PtNi	1 mol/L NaOH + 3.5 at.% NaCl	22	38	Chem. Mater. 2023, 35, 8529-8539.
Pt/CNT-$_{100}(N_2H_5)_4Mo_2S_6$	1 M KOH + seawater	20	32.8	Appl. Catal. B-environ. 2023, 338. 122996.
Co/Co_9S_8/1000	alkaline seawater	136.2	118.8	Int. J. Hydrogen Energ. 2023, 48, 29583-29592.

Table S7. Photovoltaic solar-cell-driven electrolysis measurements results of Pt/C, Pt networks, Pt_3Ni networks, $Pt_3Ni_{2-3x}@(Ni_3B)_x$, and $Pt_2Ni_{3-3x}@(Ni_3B)_x$.

Sample	Volume of H_2 (mL)	Volume of O_2 (mL)	Current (mA)	STH
Pt/C	20	10.5	39.3	11.8%
Pt networks	18.5	9.5	38.3	12.2%
Pt_3Ni networks	21.5	10.5	43.5	13.4%
$Pt_3Ni_{2-3x}@(Ni_3B)_x$	24	12	48.1	14.8%
$Pt_2Ni_{3-3x}@(Ni_3B)_x$	22.5	11	44.6	13.7%

Table S8. ICP analysis of the Pt and Ni concentration in electrolyte for Pt_3Ni networks and $Pt_3Ni_{2-3x}@(Ni_3B)_x$ during 20 hours of HER chronoamperometric test at 100 mA cm^{-2}.

	Pt_3Ni networks ($mg\ L^{-1}$)		$Pt_3Ni_{2-3x}@(Ni_3B)_x$ ($mg\ L^{-1}$)	
	Pt	Ni	Pt	Ni
2 hours	0.41	0.18	0.06	0.11
4 hours	0.67	0.32	0.07	0.20
6 hours	0.85	0.41	0.09	0.31
8 hours	1.05	0.52	0.12	0.37
10 hours	1.18	0.54	0.17	0.44
12 hours	1.24	0.57	0.22	0.45
14 hours	1.33	0.57	0.23	0.50
16 hours	1.35	0.58	0.24	0.50
18 hours	1.36	0.59	0.24	0.51
20 hours	1.36	0.59	0.25	0.52

Reference

(1) Fang, F.; Wang, Y.; Shen, L. W.; Tian, G.; Cahen, D.; Xiao, Y. X.; Chen, J. B.; Wu, S. M.; He, L.; Ozoemena, K. I.; Symes, M. D.; Yang, X. Y. Interfacial Carbon Makes Nano-Particulate RuO2 an Efficient, Stable, pH-Universal Catalyst for Splitting of Seawater. Small 2022, 18, e2203778.

(2) Hafner, J. Ab-initio simulations of materials using VASP: Density-functional theory and beyond. J. Comput. Chem., 2008, 29, 2044–2078.

(3) Perdew, J. P.; Burke, K.; Ernzerhof, M. Generalized Gradient Approximation Made Simple. Phys. Rev. Lett., 1996, 77, 3865–3868.

(4) Blöchl, P. E. Projector augmented-wave method. Phys. Rev. B, 1994, 50, 17953–17979.

(5) Grimme, S.; Antony, J.; Ehrlich, S.; Krieg, H. A consistent and accurate ab initio parametrization of density functional dispersion correction (DFT-D) for the 94 elements H-Pu J. Chem. Phys., 2010, 132, 154104.